Journal of Materials Chemistry B

PAPER

View Article Online
View Journal | View Issue

Cite this: J. Mater. Chem. B, 2018, 6, 6808

Bioceramic microneedle arrays are able to deliver OVA to dendritic cells in human skin

Helen Vallhov, [a] Wei Xia, [b] Håkan Engqvist [b] and Annika Scheynius *[ac]

Received 5th June 2018,
Accepted 13th September 2018

DOI: 10.1039/c8tb01476k

rsc.li/materials-b

Microneedle-based vaccination into skin has several advantages over vaccination using conventional needles for intramuscular or subcutaneous injections. Microneedle (MN) arrays allow the vaccine to be delivered in a minimally invasive manner and directly into the skin, whereby the skin's superficial immune cells are not by-passed. Additionally, a systemic distribution of the vaccine may be avoided, which implies less side effects and less amount of vaccine needed. For a successful delivery, the needles need to penetrate the stratum corneum and reach the potent network of antigen-presenting dendritic cells (DCs). In this study, we evaluated patches covered with biodegradable ceramic (calcium sulphate) MNs with a tip diameter of approximately 3 μm and with two different lengths (300 and 600 μm) for their ability to penetrate and transfer the model allergen ovalbumin (OVA) into epidermis. MNs with a length of 600 μm (MN-600) and a volume average pore size of 12 ± 1 μm were more efficient in crossing the stratum corneum and to deliver OVA into $CD1a^+$ DCs residing in the epidermis of human *ex vivo* skin, in comparison to MNs with a length of 300 μm. Quantitative *in vitro* release studies showed that approximately 90% of the loaded OVA could be released from MN-600 within 1 h. These findings support the further development of ceramic MNs for transcutaneous immunization.

Introduction

Today, intramuscular injection is the most common vaccine delivery method. However, it has several disadvantages including inoculation needing professionals, sharp needle disposal, infection, the requirement for cold-chain distribution, and the relatively low density of immune cells at the muscle site.[1,2] To overcome these drawbacks, a range of novel delivery methods are being developed, including microneedle (MN) arrays.[3] Using MNs as vaccine carriers is highly beneficial for a wide range of vaccinations due to increased stability of vaccines, less sensitivity to temperature changes, and ease of administration.[4] In addition, MN technology offers an efficient, minimally invasive, and potentially pain free delivery of the vaccine into the upper layer of the skin, epidermis, which contains a network of dendritic cells (DCs).[5] These cells are among the first cells to encounter foreign substances, whereby they migrate from their peripheral sites with their cargo to regional lymph nodes. Here, DCs have an exceptional capacity to interact with T cells and B cells by expressing different co-stimulatory molecules and cytokines, and depending on the type of stimulus, they can initiate primary and secondary immune responses or induce tolerance.[6,7]

MN arrays have previously been shown to be efficient in targeting vaccine into the skin, where they are able to induce improved immune responses compared to intramuscular injection. Thus, a 100-fold lower dose of a conventional influenza vaccine was sufficient in a mouse model when delivered *via* MNs.[8] In addition, by using MNs, a solid formulation of the vaccine can be used, which allows cold-chain free transportation and storage.[3]

To achieve an efficient delivery of the vaccine into epidermis, the length of the MNs needs to be optimized. They need to be long enough to pierce the outermost layer of skin, the stratum corneum, to overcome the elasticity of the skin, but short enough to avoid stimulation of nerve endings located in dermis or bleeding. Also the sharpness of the needle tip and whether an applicator is used affect the ease of penetration.[1,9] Furthermore, the choice of material and structural shape is crucial. Most currently explored MNs are Si, metal or polymer based. These concepts all represent non-resorbable alternatives, *i.e.* they are not intended to stay in the skin after insertion.[10,11] Silicon MNs were primarily used due to their sharpness,[10] but studies showed that the material is too brittle with the risk of leaving broken needles in the skin, which could induce inflammation.[10] Metal MNs have favourable mechanical properties, but still there is a risk of leaving non-biocompatible residues in the skin, and the manufacturing cost is relatively high at bulk volumes due to expensive raw materials and

[a] Department of Clinical Science and Education, Karolinska Institutet, and Sachs' Children and Youth Hospital, Södersjukhuset, SE-118 83 Stockholm, Sweden. E-mail: Annika.scheynius@ki.se; Tel: +46 (0)70 6057927
[b] Division for Applied Materials Science, Department of Engineering Sciences, The Ångström Laboratory, Uppsala University, SE-751 21 Uppsala, Sweden
[c] Science for Life Laboratory, Clinical Genomics, Karolinska Institutet, SE-171 77 Stockholm, Sweden

manufacturing processes.[10,11] Furthermore, drug loading is limited to coating techniques.[10]

There are two options for resorbable MNs, either biodegradable polymers or ceramics. As a comparison with metals, polymeric MNs are relatively inexpensive and are amenable for mass production.[10,12] In addition, drugs may be incorporated into the polymers to achieve controlled drug delivery.[1] Previous studies have highlighted the use of polymeric MNs, which can be dissolved, thereby avoiding sharp waste and allowing an efficient transfer of the vaccine.[13] However, the high temperature processing or use of organic solvents (difficult to load active ingredients) and the relatively low mechanical strength of biodegradable polymers (difficult to penetrate the elastic skin) limit the use of synthetic biodegradable polymers.[10,14,15] Thus, biodegradable bioceramic materials are often more suitable for skin penetration.[10] Bioceramics have been shown to be a promising material for use in MNs, also due to good *in vivo* resorbability,[16] adjustable porosity, high mechanical strength[17] and controlled drug release.[18] Ceramic MNs prepared by a traditional sintering technique are generally oxides, such as alumina, which have limited drug loading capacity.[19] Bigger pores in *e.g.* sintered alumina could result in very blunt tips combined with low mechanical strength of the needles. Most sintered ceramics are also non-resorbable and if the needles would brake during insertion they could cause unwanted effects in the skin (*e.g.* irritation, inflammation). Thus, there is a need to find MNs with high mechanical strength, but simultaneously with a high loading capacity and preferably also biodegradable.

Well-known self-setting and biodegradable bioceramics, such as calcium sulphate dihydrate [gypsum ($CaSO_4{\cdot}2H_2O$); CaS] and calcium phosphates [brushite ($CaHPO_4{\cdot}2H_2O$) and apatite; CaP] are promising materials, which have been validated as bone substitution materials in several *in vivo* and clinical tests.[16,20–22] We have previously developed calcium sulphate dihydrate and brushite needles that have high mechanical strength and are biodegradable,[17] which may promote safe and efficient transdermal drug delivery. In addition, their adjustable porosity and electrostatic interactions are favorable to achieve controlled drug release.[17] Previously, we have demonstrated the ability of these ceramic MNs to be loaded with a drug under mild conditions (room temperature, neutral pH and ambient pressure), and how the release rate could be controlled by the surface area, porosity and resorption rate of the ceramic needles.[17] We have also assessed the penetration of calcium sulphate dihydrate MNs with heights of 450 μm and 600 μm and a tip radius of about 5 μm into pre-frozen porcine skin from the ear.[18] However, the stratum corneum of porcine ear skin is thinner, around 10 μm, compared to human skin, where the thickness of the stratum corneum of the upper arm is around 17 μm and even up to 35 μm for abdominal skin.[23,24]

To ascertain full penetration through human skin in order to reach the epidermis, we therefore in this study optimized the ceramic MNs with increased sharpness and compared different lengths of the needles, and evaluated them on human *ex vivo* skin for their ability to deliver a cargo to dendritic cells.

Materials and methods

Fabrication of bioceramic MNs

Two master moulds for the MNs were prepared by Ginolis (Oulu, Finland) with different heights of the needles to test the possibility to reach the epidermis after penetrating the stratum corneum: (1) one mould containing 300 μm high MNs (denoted as MN-300), and (2) another mould containing 600 μm high MNs (denoted as MN-600), both with a base width of 300 μm. The number of microneedles on each MN-300 and MN-600 was 50 and 25, respectively (Fig. 1). A negative replica mould of the master mould was prepared using silicone rubber (Fig. 1). The size of each patch was 0.5 × 0.5 cm. Alpha calcium sulphate hemihydrate ($CaSO_4{\cdot}0.5H_2O$, α-CSH) was bought from Bo Ehrlander AB, Munkedal, Sweden. The raw α-CSH was sieved to get particle sizes of less than 100 μm, which resulted in an average particle size of 26.3 μm ($D(4,3)$), the volume mean diameter, as measured using a Malvern system (Mastersizer 3000, Malvern Panalytical, UK). The sieved α-CSH was then mixed (by hand using a spatula) with deionized water, in a liquid/powder ratio of 0.45, to form a homogeneous paste. The paste was filled into the mould and cured for 5 h at room temperature.

Characterization of bioceramic MNs

The crystal phases of the MNs were analyzed by X-ray diffraction (D8 ADVANCE, Bruker AXS GmbH, Germany). The morphology and size of the prepared bioceramic MNs (MN-300 and MN-600) were analyzed by scanning electron microscopy (SEM, LEO 1550, Zeiss, UK). Due to the small size of the needles, pore size analyses of the bioceramic MNs were performed by micro-computed tomography (microCT; Bruker AXS GmbH). The bulk porosity, BET and *z*-potential have been published earlier.[17,25] The tip diameter was estimated from microCT and SEM analysis.

Human skin explants

Human skin explants were chosen to evaluate the penetration ability of the ceramic MNs. Abdominal skin from the leftovers after performing cosmetic surgery at local hospitals from 6 donors was stored at 4 °C and taken care of within 24 h. After the fat was trimmed off, the skin was stretched onto a cork plate covered with parafilm. The surface of the skin was washed with PBS and ethanol and allowed to reach room temperature before experiments. This work was approved by the regional ethical review board in Stockholm (2015/2082-31/1), and written informed consent was obtained from all subjects donating skin. All experiments were performed in accordance with the ethical principles for medical research in the Helsinki Declaration.

Ex vivo skin penetration

MN-300 and MN-600 were pressed manually for 1 min onto stretched human *ex vivo* skin, and thereafter punch biopsies (0.5 cm in diameter) were taken at the center of the treated site expanding the whole thickness of the skin, snap-frozen and stored at −80 °C (Fig. 2A). Non-treated skin was used as the control. Thereafter, 20 μm-thick cryosections from each

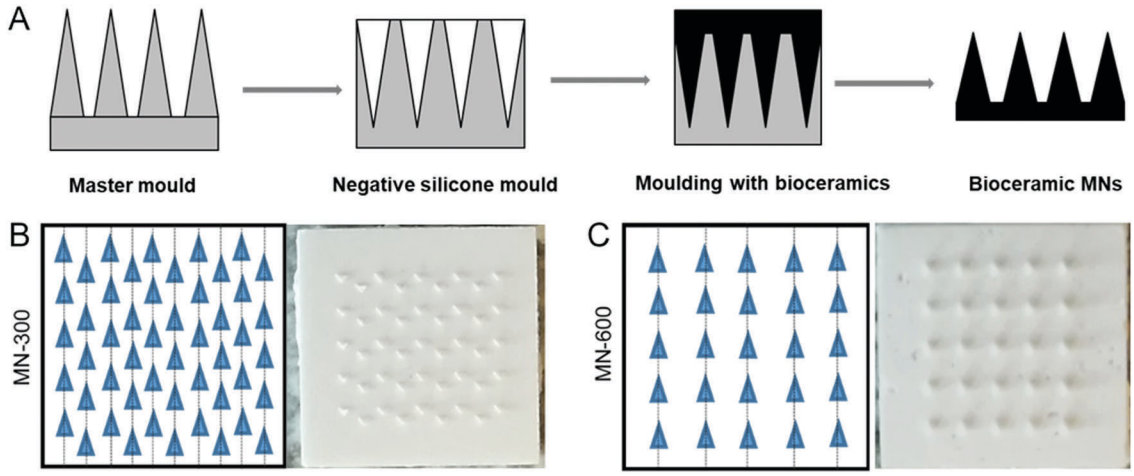

Fig. 1 (A) Illustration of the micro-moulding process used in the preparation of bioceramic MNs. (B) The drawing and pictures of 50 needles of MN-300 and (C) 25 needles of MN-600. The size of each patch is 0.5 × 0.5 cm.

specimen were prepared, followed by routine hematoxylin and eosin staining, and analysed by microscopy (Olympus BX51, PA, USA). The percentage of broken needles on the patches after insertion into the skin was analysed by SEM, and calculated to be $(N_0 - N_b)/N_0 \times 100\%$. N_0 is the original number of needles on each patch. N_b is the number of broken needles on each patch after skin penetration. The broken needles include the needles with broken tips and totally disappeared needles.

In order to verify the penetration ability of the two different ceramic MNs into skin, a trypan blue assay was performed (Fig. 2B).[9,26] The MNs were manually pressed on the skin for 1 min and thereafter 30 μl of 0.4% trypan blue (Bio-Rad, Hercules, CA, USA) was applied onto the site of treated skin for 1 h.

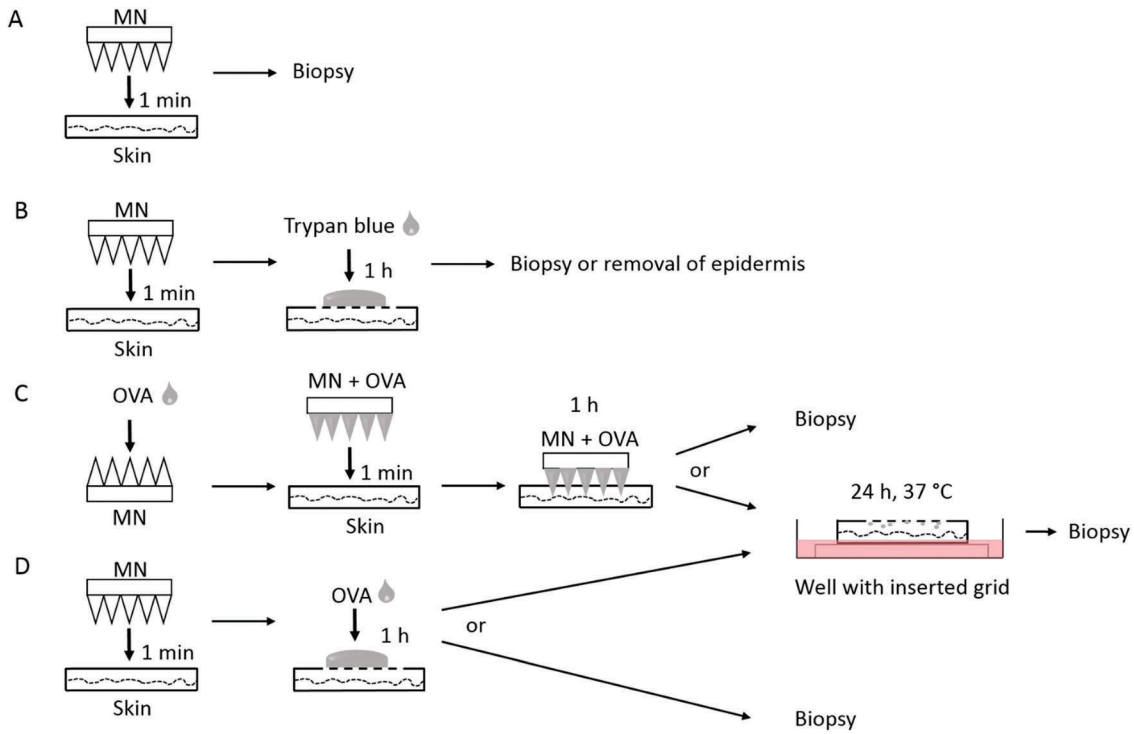

Fig. 2 Illustration of penetration experiments with bioceramic microneedles (MNs) on human *ex vivo* skin. (A) MNs were pressed manually onto the skin for 1 min, whereafter a biopsy was taken. (B) A drop of trypan blue was added onto the pierced skin and left for 1 h and thereafter a biopsy was taken or epidermis was removed. (C) OVA-coated MNs were pressed manually onto the skin for 1 min, left on the skin for 1 h, and thereafter a biopsy was taken, or the skin was further incubated at 37 °C for 24 h before a biopsy was taken. (D) Non-coated MNs were manually pressed for 1 min onto the skin, removed, and thereafter a drop of OVA was added onto the pierced skin for 1 h and thereafter a biopsy was taken, or the skin was further incubated at 37 °C for 24 h before a biopsy was taken.

Residual trypan blue was washed away from the surface by using PBS. Biopsies (0.5 cm in ∅) were taken at the center of the treated site expanding the whole thickness of the skin, snap-frozen and stored at −80 °C. Cryostat sections, 20 μm thick, from each skin biopsy specimen were processed for routine eosin staining. Stained sections were observed by microscopy (Olympus BX51). Furthermore, the stratum corneum side of the treated skin was photographed. Thereafter, the epidermis was heat separated from the dermis at 60 °C for 2 min, and the upper dermis side was photographed.

Delivery of ovalbumin into the skin

MN-600 was coated with 30 μl of a solution containing 30 μg ovalbumin (OVA) conjugated with Alexa 488 (Invitrogen, Thermo Fisher Scientific, Waltham, MA, USA) and air-dried. Thereafter they were manually pressed for 1 min onto the stretched skin, pre-cut into 2 × 2 cm pieces, and left on the skin for 1 h at room temperature (Fig. 2C). Then the skin was washed with PBS and punch biopsies (0.5 cm in ∅) were taken at the center of the treated site expanding the whole thickness of the skin, or the skin was further incubated at 37 °C for 24 h (Fig. 2C). Here, the skin specimens were placed on grids (3 cm in ∅) inserted into 6 well plates (Falcon, Corning, NY, USA) containing 2 ml RPMI 1640 medium (Gibco, Thermo Fisher Scientific) and supplemented with 2 mM L-glutamine (Gibco, Thermo Fisher Scientific), 100 IU ml^{-1} penicillin, 100 μg ml^{-1} streptomycin, 50 μM β-mercaptoethanol, and 10% heat inactivated fetal calf serum (HyClone, South Logan, UT, USA), ensuring the skin to have contact with media. Thereafter, the skin surface was washed with PBS, and punch biopsies were taken as above. Alternatively, non-coated MNs was manually pressed for 1 min onto the skin, removed and thereafter a drop of 30 μl containing 30 μg OVA-Alexa 488 was applied onto the pierced skin (Fig. 2D). After 1 h at room temperature, the skin was washed with PBS and biopsies were taken, or the skin was further incubated at 37 °C for 24 h in a similar way as above followed by taking punch biopsies (Fig. 2D). As a control, a droplet of 30 μl containing 30 μg OVA-Alexa 488 was applied onto the top of non-pierced skin and incubated at 37 °C for 24 h as above. Thereafter, the skin was washed with PBS and punch biopsies were taken. All biopsies were snap-frozen and stored at −80 °C.

For the analysis of the delivery of OVA into the skin, 20 μm-thick cryostat sections were prepared from the biopsies and fixed in cold acetone/H_2O 1 : 1 for 30 s, followed by 5 min in 100% acetone. After washing with PBS, the samples were stained with mouse anti-human CD1a (BD Biosciences, Franklin Lakes, NJ, USA) followed by Alexa Fluor 555 anti-mouse IgG (Invitrogen). Slides were mounted with Vectashield Antifade Mounting Medium (Vector Laboratories, Burlingame, CA, USA), and images of the planes at varying depths within the skin sections (z-scans) were acquired by using confocal microscopy (TCS SP2; Leica Microsystems, Mannheim, Germany).

Quantitative analysis of released OVA

To quantify the release of OVA loaded onto MN-600 arrays, the MNs were soaked in phosphate buffered saline (PBS) at 2 ml per MN at room temperature. The MNs were removed after 10 min, 30 min, and 1 h, and thereafter dried at 40 °C over night. Each MN array was cut with a sharp knife and split into 9 pieces

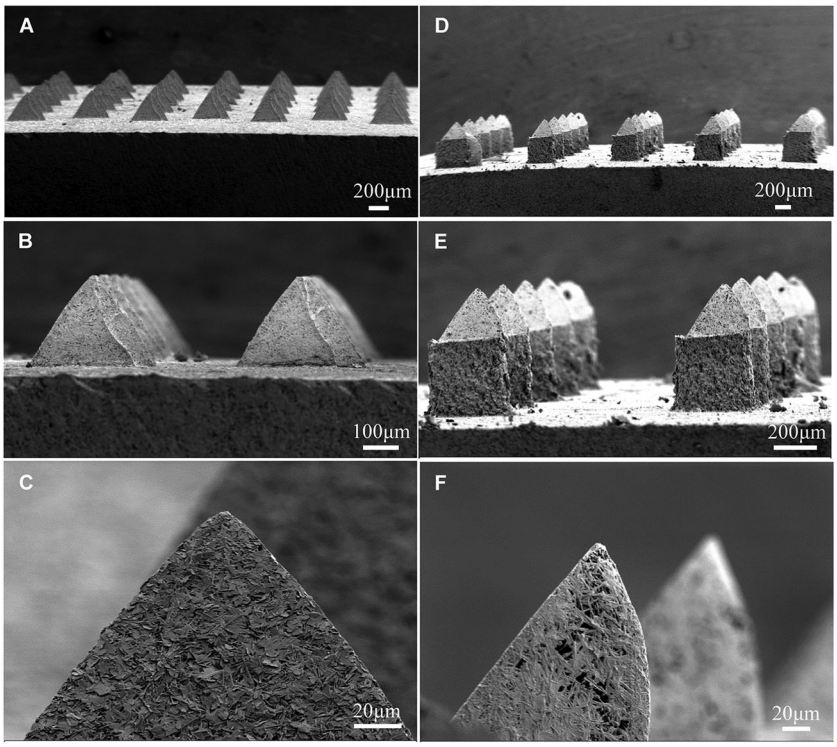

Fig. 3 Morphology and structure of two bioceramic MNs. (A–C) Scanning electron microscopy (SEM) images of MN-300 and (D–F) of MN-600: increased magnification of the needles from top to bottom. (C) and (F) seen from different angles.

before further analysis to achieve several data points from the same MN array over time. The weight of OVA left in the MN arrays ($n = 3$) was analyzed by thermogravimetric analysis (TGA, TGA/DSC 3+ and TGA/SDTA 851e, Mettler-Toledo, Greifensee, Switzerland), whereby the release of OVA into PBS could be estimated. The analyses were performed in aluminum pans between 25 and 600 °C at 5 °C min^{-1} under an air atmosphere.

Results

Characterization of bioceramic MN-300 and MN-600

The pyramid shape of the needles was similar for MN-300 and MN-600, with a tip diameter of approximately 3 μm (Fig. 3). The higher magnification of the SEM images indicated that the MNs were porous (Fig. 3C and F). The pore size of MN-300 varied from 1.5 μm to 22.4 μm, and the volume average pore size was 11 ± 2 μm ($n = 3$). The pore size of MN-600 varied from 1.5 μm to 37.4 μm, and the volume average pore size was 12 ± 1 μm ($n = 3$), see Fig. 4. Thus the pore size distribution and volume average were similar for both MN arrays. The X-ray diffraction patterns (Fig. 5) show that both MN-300 and MN-600 mainly contained gypsum–calcium sulphate dihydrate with some residues of unreacted bassanite–calcium sulphate hemihydrate from the precursor powder.

Penetration ability of the MNs

We used human *ex vivo* skin and applied the MN patches under manual pressure for 1 min. Biopsy specimens indicated that MNs were able to cross the stratum corneum, which was seen with both MN-300 and MN-600 μm (Fig. 6). To confirm the piercing ability of the MNs, a low-molecular weight model compound, trypan blue, was added on top of the treatment site for 1 h. Traces of trypan blue in epidermis verified the ability of the MNs to cross the stratum corneum, which was especially convincing for the needles of 600 μm length (MN-600) (Fig. 6C).

To further investigate the ability of the MNs to cross the skin, epidermis of the treated site was heat separated and removed from dermis. Trypan blue spots were observed down to the dermis demonstrating the penetration ability of the MNs, which was more evident again for the 600 μm long needles compared to the MNs with a length of 300 μm (Fig. 6D and E).

The insertion into the skin had also an impact on the MNs, where 36.4% (SD = 13.2, $n = 3$) of the needles on MN-300 was broken, and 27.5% (SD = 10.5, $n = 3$) on MN-600.

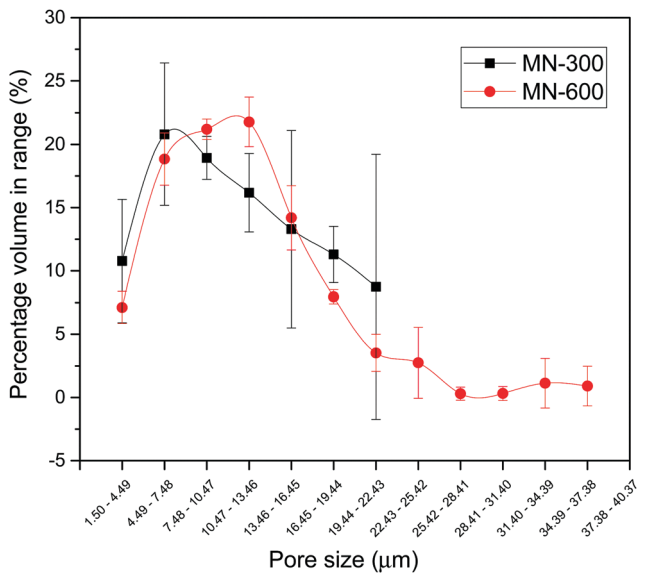

Fig. 4 Pore size distribution in the needles of MN-300 and MN-600 as determined using microCT and calculated using a sphere-fitting model in the 3D pore system (Bruker microCT). For MN-300, no pores could be detected above 22.43 mm. The data points were average ± SD for $n = 3$, with needles from the same patch, and presented as volume percentage (y-axis) within the given size range on the x-axis.

Delivery of fluorescently labeled ovalbumin into human *ex vivo* skin

Next, the delivery of the model antigen/allergen OVA, a 45 kDa bio-macromolecule, into the skin by MN-600 was investigated, which had been the MN patch that was most successful in penetrating the skin. When MN-600 coated with OVA-Alexa 488 was pressed for 1 min onto the skin and left for 1 h, traces of fluorescent OVA was seen at the penetration sites of the needles (Fig. 7A). After a 24 h incubation of the skin, a further release of OVA into epidermis was detected (Fig. 7B), and interactions of OVA and $CD1a^+$ DCs were observed (Fig. 7B). An even faster release of OVA into epidermis was achieved by first piercing the skin with non-coated MNs for 1 min and thereafter applying fluorescent labeled OVA onto the treatment site. Here, already after 1 h, an interaction was detected between OVA and $CD1a^+$ cells in epidermis (Fig. 7C), and a further spreading (Fig. 7D) and internalization of OVA by $CD1a^+$ DCs was seen after 24 h (Fig. 7E). Thus, MN-600 seems to enable the delivery of biomacromolecules into the skin. As a control, only Alexa 488 labeled OVA was applied onto non-pierced skin. Here, no penetration of fluorescence through the stratum corneum was observed, indicating that OVA was not able to cross the skin by itself (Fig. 7F).

In vitro release of ovalbumin from MNs

To evaluate the capacity of the MNs to release their cargo, we performed release studies with MN-600 coated with OVA. There was a fast release within 1 h. Approximately 43, 58 and 90 wt% of OVA were released from the MNs after 10 min, 30 min and 1 h in PBS (Fig. 8).

Discussion

In this study, we have improved biodegradable and biocompatible ceramic MNs by increasing the aspect ratio resulting in sharper tips, which were successfully able to penetrate human *ex vivo* skin and after loading with the bio-macromolecule, OVA, were able to release their cargo to $CD1a^+$ DCs residing in the skin.

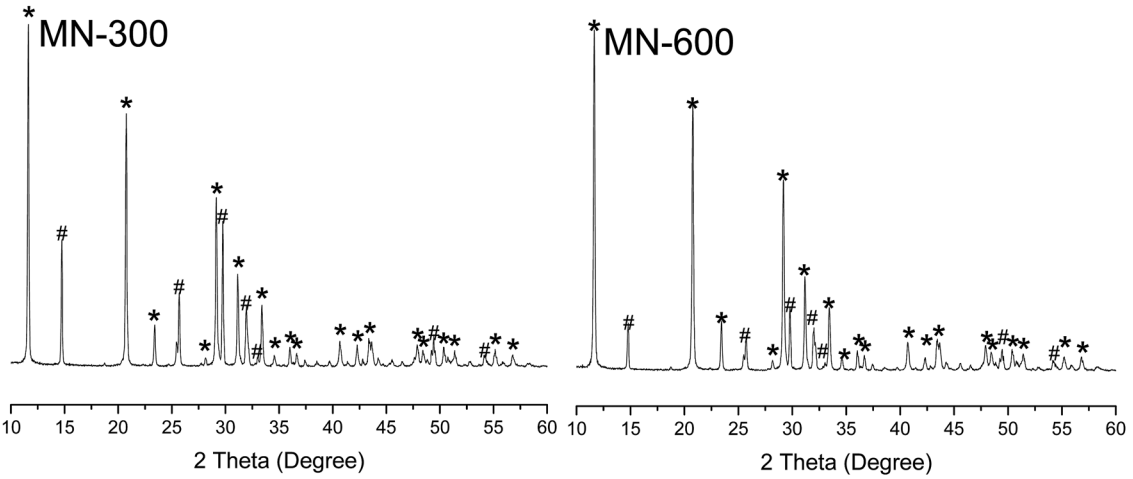

Fig. 5 X-ray diffraction (XRD) patterns of MN-300 and MN-600. *Gypsum–calcium sulphate dihydrate; #bassanite–calcium sulphate hemihydrate.

Both the shape and length of MNs are decisive if they are efficient in crossing the stratum corneum.[27] The needles need to have a sharp angle and be designed to cut through the skin easily. The elasticity of the skin hinders the penetration of short (<300 μm) MNs into the skin and often need an applicator for crossing the skin.[9,26] Previous studies also suggest that the length of the MNs influences the antigen-specific immune responses, where 200–300 μm long MNs induce lower responses than 800–1000 μm long needles.[28,29] However, with increasing length, the risk of inducing pain becomes greater.[10] Preliminary, we used ceramic MN patches with needle lengths of 450 and 600 μm and with a tip radius of 5 μm, which successfully had penetrated porcine skin.[17] We found, however, that these MN patches were not able to pierce human *ex vivo* skin (results not shown), which may be due to the thicker stratum corneum of human skin compared to porcine skin.[23,24] We therefore evaluated two new master moulds, which resulted in MNs with a decreased tip diameter down to 3 μm, and with a needle length of 300 μm or 600 μm to explore if we were able to penetrate into epidermis without the use of an applicator. We here demonstrated that MN-600 was successful and more efficient in penetrating the skin and reaching down to epidermis compared to MN-300 (Fig. 6C). A few needles seemed to be able to even reach below epidermis as shown in Fig. 6E, but which was not observed in the cryo-sections (Fig. 6C and 7A–D), indicating a very shallow penetration into dermis with a low risk of inducing pain.

Ceramic material is hard, but also brittle. For both MN-300 and MN-600, about 30% of the needles or parts of the needles were broken during insertion, which may be due to an uneven manual application. Most broken tips were found on the surface of the skin (data not shown), but even if they were inserted into the skin they pose a low risk due to the good *in vivo* resorbability of the bio-ceramics.[17,30]

Ceramic MNs can easily be prepared with dry vaccine coatings, which can be applied under gentle conditions at room temperature. Dry vaccine is more stable compared to when dissolved in liquids, and following application they can rapidly dissolve within the skin.[31] Due to the ability to adjust the porosity of the bioceramic material, they can act as carriers for bio-macromolecules such as vaccines (typical molecular sizes of soluble antigens are 1–10 nm[32]) and the loading capacity can even be enhanced if the vaccine is moulded into the MNs during the production process.[18] The calcium sulphate used in this study (hemihydrate precursor powder that reacts into dehydrate after hardening) forms a relatively porous outer surface (see Fig. 3). To measure the porosity and pore size distribution of surfaces can be difficult, and here we choose to use microCT because it can be site specific (although the pores that can be detected with the technique need to be above about 1 μm). We found that MN-300 and MN-600 have similar volume average pore sizes and pore size distributions (Fig. 4). As a comparison, the overall porosity of calcium sulphate has been determined to about 40 vol%, the surface area (BET) to 27.1 $m^2 g^{-1}$ and the zeta potential of calcium sulphate particles in 0.05 M NaCl solution at pH = 6.8 was −15.74 mV.[17,25]

There are several different approaches for the transdermal drug delivery by MNs.[33] In this study, we compared two strategies for delivering OVA (fluorescently labeled) into skin: one using MN-600 coated with OVA before application onto the skin (Fig. 2C), and another strategy where the skin was first pierced with MN-600 and thereafter a droplet of OVA was applied onto the skin (Fig. 2D). The latter method has the disadvantage of needing a two-step administration process, but by coating the MNs, there is also a risk of reducing the sharpness of the needles.[1] Our results showed a successful delivery of OVA into the skin by both approaches (Fig. 7A–E). A faster release and uptake in $CD1a^+$ DCs was seen by first piercing the skin with MNs and thereafter applying OVA on top of the skin, thus depending on the demand of a quick or delayed release, different strategies may be used. An even more delayed release may be achieved by incorporating the cargo within the MNs, which then is released while MNs are biodegraded in the skin,[17] but this requires that the needles

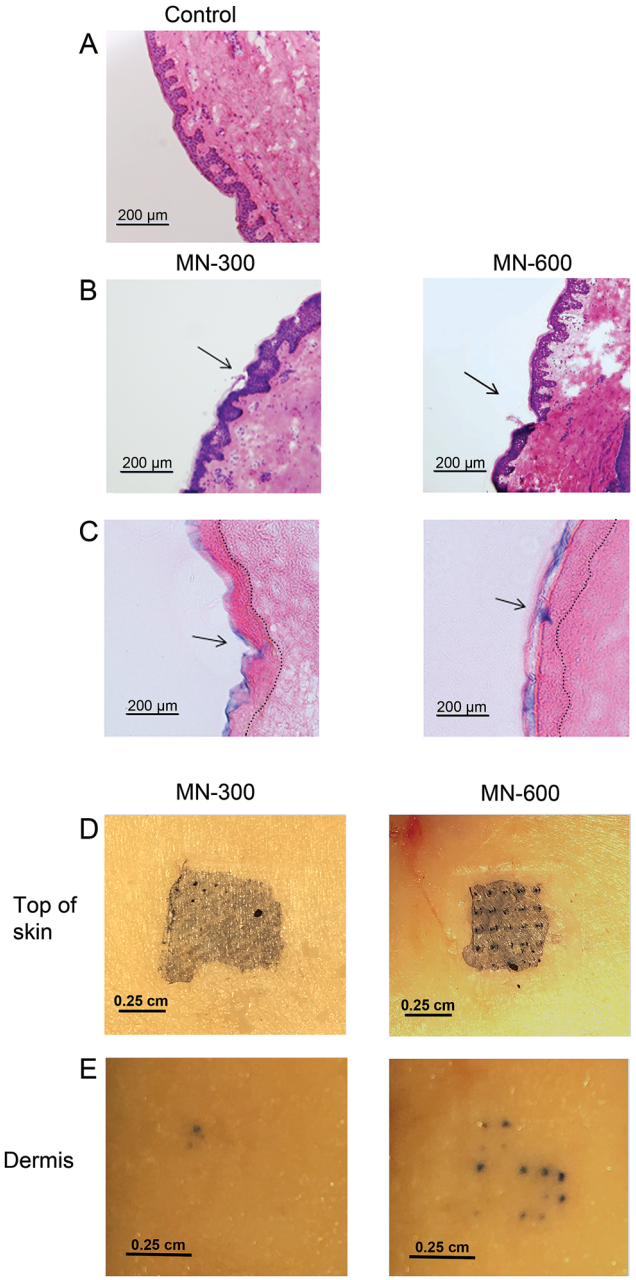

Fig. 6 Ceramic MNs with a length of 600 μm are more efficient in crossing the stratum corneum than MNs with a length of 300 μm. Hematoxylin and eosin staining of cryo-sections (20 μm thick) of human skin samples. (A) Non-treated skin *versus* skin where (B) MN-300 or MN-600 had been manually pressed onto the skin for 1 min (n = 1). (C) Eosin staining of cryo-sections (20 μm thick) of skin samples where MN-300 and MN-600 had been pressed onto the skin for 1 min, and thereafter a droplet of trypan blue was added for 1 h onto the site of treatment. (D) Skin samples where MN-300 or MN-600 had been manually pressed onto the skin for 1 min, followed by the addition of trypan blue for 1 h, revealed the spots of trypan blue down to dermis, which (E) became visible after the removal of epidermis. Images in C–E are representatives of experiments with skin from three different donors.

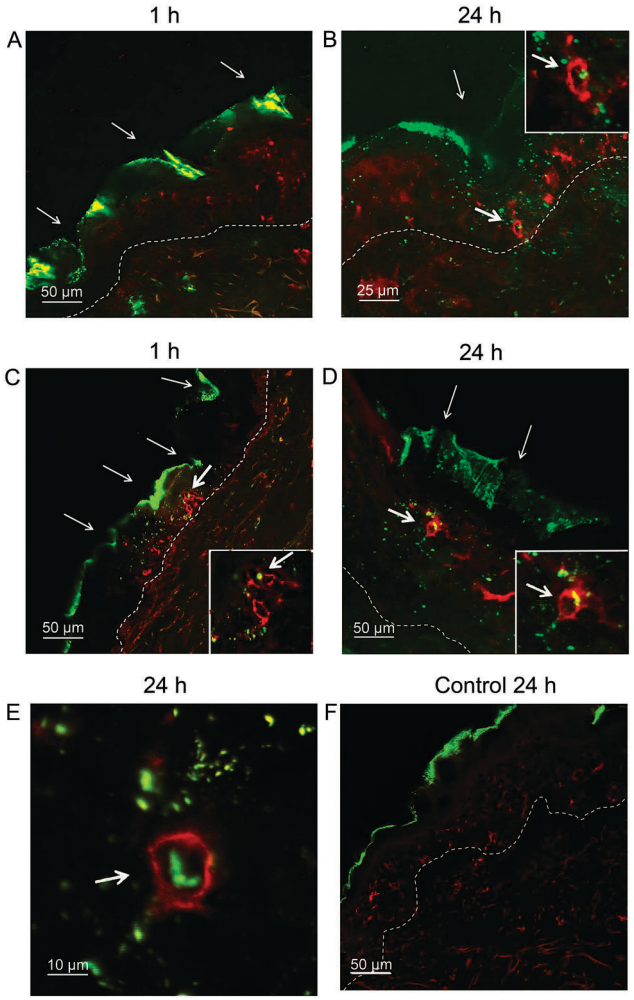

Fig. 7 MN-600 enables the delivery of OVA to CD1a$^+$ cells in epidermis. CLSM analyses of cryo-sections (20 μm thick) of human *ex vivo* skin specimens (A) where OVA-Alexa 488 (green) coated MNs with a length of 600 μm had been manually pressed for 1 min onto the skin and then left on the skin for 1 h, and (B) where skin treated as in A was further incubated at 37 °C for 24 h. (C) Skin, onto which non-coated MN-600 had been manually pressed for 1 min, was removed and thereafter a drop of 30 μl containing 30 μg OVA-Alexa 488 (green) had been applied onto the pierced skin for 1 h, and (D) skin treated as in C but which was further incubated at 37 °C for 24 h. (E) Z-scan to show internalization of OVA into a CD1a$^+$ cell in the epidermis skin treated as in D. (F) Skin which had only been treated with a drop of 30 μg OVA-Alexa 488 (green) on the surface for 24 h at 37 °C as a control. Narrow arrows indicate the insertion marks of MNs into the skin. Bold arrows indicate CD1a$^+$ cells (red) interacting with OVA (green), when overlapped as in D is visible in yellow. Higher magnification images are shown as insets in (B–D). Dashed lines indicate the borderline between epidermis (upper part) and dermis (below). The images shown are representatives of experiments with skin from two different donors.

are left in the skin for a longer time period. Hereby, a positive depot effect may be achieved, which may enhance the efficacy of the vaccine as demonstrated for OVA-encapsulated chitosan MNs applied on rats.[34]

Quantitative release studies indicated a 90 wt% release of OVA from the MNs within 1 h (Fig. 8) in line with our confocal microscopy studies, which demonstrated traces of released OVA in skin after 1 h (Fig. 7A). In comparison, Maaden *et al.* showed a release efficiency of 70% into *ex vivo* human skin, studying OVA-coated silicon MN arrays.[35] Further adjustments of the release can be achieved by changing the bulk surface area, porosity and resorbability of the ceramics.

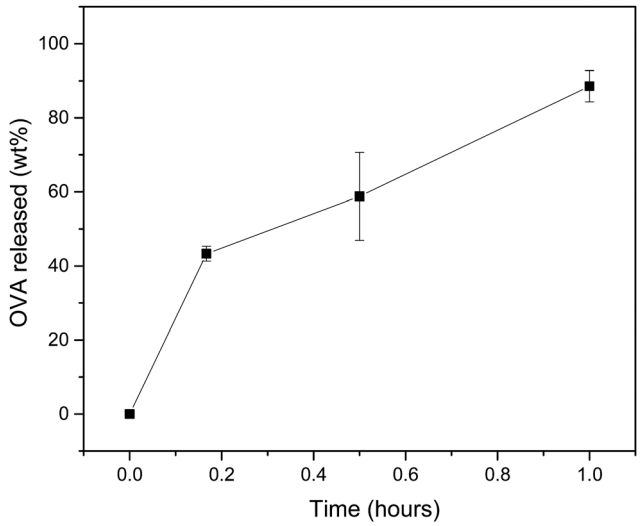

Fig. 8 OVA released from MN-600 in PBS during 1 h at room temperature as measured by thermogravimetric analysis (TGA). Results represent mean ± SD of the fraction of OVA released from the MNs (n = 3 different experiments).

Conclusions

In this study, an improved bioceramic MN array with a high-aspect-ratio needle was prepared. This design allowed the MN-600 array to penetrate human *ex vivo* skin and to deliver its cargo to $CD1a^+$ DCs in epidermis. Our study suggests that bioceramic MNs have potential application within MN-based vaccination.

Conflicts of interest

Engqvist is the co-inventor to a patent covering bioceramic microneedles owned by Emplciure AB.

Acknowledgements

We thank Catharina Johansson, Karolinska Institutet, for assistance with skin preparations, Caroline Öhman Mägi and Song Chen, Uppsala University, for assistance with microCT, and the NANOASIT members for fruitful discussions. We also thank Strandkliniken, Stockholm, and their patients for supplying us with skin. AS was supported by grants from the Swedish Research Council, the Cancer and Allergy Association, and through the regional agreement on medical training and clinical research (ALF) between the Stockholm County Council and the Karolinska Institutet. HV was supported by grants from the Hesselman Foundation and by HKH Kronprinsessan Lovisas förening. HE, WX, and AS were supported by NANOASIT II (ERA-NET EuroNanoMed II).

References

1 K. van der Maaden, W. Jiskoot and J. Bouwstra, Microneedle technologies for (trans)dermal drug and vaccine delivery, *J. Controlled Release*, 2012, **161**(2), 645–655.
2 A. P. Raphael, M. L. Crichton, R. J. Falconer, S. Meliga, X. Chen and G. J. Fernando, *et al.*, Formulations for microprojection/microneedle vaccine delivery: Structure, strength and release profiles, *J. Controlled Release*, 2016, **225**, 40–52.
3 T. Wang and N. Wang, Biocompatible Mater Constructed Microneedle Arrays as a Novel Vaccine Adjuvant-Delivery System for Cutaneous and Mucosal Vaccination, *Curr. Pharm. Des.*, 2015, **21**(36), 5245–5255.
4 J. W. Li, M. T. Zeng, H. Shan and C. Y. Tong, Microneedle Patches as Drug and Vaccine Delivery Platform, *Curr. Med. Chem.*, 2017, **24**(22), 2413–2422.
5 X. N. Wang, N. McGovern, M. Gunawan, C. Richardson, M. Windebank and T. W. Siah, *et al.*, A three-dimensional atlas of human dermal leukocytes, lymphatics, and blood vessels, *J. Invest. Dermatol.*, 2014, **134**(4), 965–974.
6 J. Banchereau and R. M. Steinman, Dendritic cells and the control of immunity, *Nature*, 1998, **392**(6673), 245–252.
7 S. Yamazaki, K. Inaba, K. V. Tarbell and R. M. Steinman, Dendritic cells expand antigen-specific Foxp3+ CD25+ CD4+ regulatory T cells including suppressors of alloreactivity, *Immunol. Rev.*, 2006, **212**, 314–329.
8 G. J. Fernando, X. Chen, T. W. Prow, M. L. Crichton, E. J. Fairmaid and M. S. Roberts, *et al.*, Potent immunity to low doses of influenza vaccine by probabilistic guided micro-targeted skin delivery in a mouse model, *PLoS One*, 2010, **5**(4), e10266.
9 K. van der Maaden, E. M. Varypataki, H. Yu, S. Romeijn, W. Jiskoot and J. Bouwstra, Parameter optimization toward optimal microneedle-based dermal vaccination, *Eur. J. Pharm. Sci.*, 2014, **64**, 18–25.
10 Y. C. Kim, J. H. Park and M. R. Prausnitz, Microneedles for drug and vaccine delivery, *Adv. Drug Delivery Rev.*, 2012, **64**(14), 1547–1568.
11 K. Ita, Transdermal Delivery of Drugs with Microneedles-Potential and Challenges, *Pharmaceutics*, 2015, **7**(3), 90–105.
12 M. J. Garland, K. Migalska, T. M. Mahmood, T. R. Singh, A. D. Woolfson and R. F. Donnelly, Microneedle arrays as medical devices for enhanced transdermal drug delivery, *Expert Rev. Med. Devices*, 2011, **8**(4), 459–482.
13 T. M. Tuan-Mahmood, M. T. McCrudden, B. M. Torrisi, E. McAlister, M. J. Garland and T. R. Singh, *et al.*, Microneedles for intradermal and transdermal drug delivery, *Eur. J. Pharm. Sci.*, 2013, **50**(5), 623–637.
14 W. Yu, G. Jiang, D. Liu, L. Li, Z. Tong and J. Yao, *et al.*, Transdermal delivery of insulin with bioceramic composite microneedles fabricated by gelatin and hydroxyapatite, *Mater. Sci. Eng., C*, 2017, **73**, 425–428.
15 E. Larraneta, R. E. M. Lutton, A. D. Woolfson and R. F. Donnelly, Microneedle arrays as transdermal and intradermal drug delivery systems: Materials science, manufacture and commercial development, *Mater. Sci. Eng., R*, 2016, **104**, 1–32.
16 M. Bohner, Resorbable biomaterials as bone graft substitutes, *Mater. Today*, 2010, **13**(1-2), 24–30.
17 B. Cai, W. Xia, S. Bredenberg and H. Engqvist, Self-setting bioceramic microscopic protrusions for transdermal drug delivery, *J. Mater. Chem. B*, 2014, **2**(36), 5992–5998.

18 B. Cai, W. Xia, S. Bredenberg, H. Li and H. Engqvist, Bioceramic microneedles with flexible and self-swelling substrate, *Eur. J. Pharm. Biopharm.*, 2015, **94**, 404–410.
19 M. Verhoeven, S. Bystrova, L. Winnubst, H. Qureshi, T. D. de Gruijl and R. J. Scheper, *et al.*, Applying ceramic nanoporous microneedle arrays as a transport interface in egg plants and an *ex vivo* human skin model, *Microelectron. Eng.*, 2012, **98**, 659–662.
20 A. Oberle, F. Theiss, M. Bohner, J. Muller, S. B. Kastner and C. Frei, *et al.*, Investigation about the clinical use of brushite-and hydroxylapatite-cement in sheep, *Schweiz. Arch. Tierheilkd.*, 2005, **147**(11), 482–490.
21 D. Stubbs, M. Deakin, P. Chapman-Sheath, W. Bruce, J. Debes and R. M. Gillies, *et al.*, In vivo evaluation of resorbable bone graft substitutes in a rabbit tibial defect model, *Biomaterials*, 2004, **25**(20), 5037–5044.
22 F. Theiss, D. Apelt, B. A. Brand, A. Kutter, K. Zlinszky and M. Bohner, *et al.*, Biocompatibility and resorption of a brushite calcium phosphate cement, *Biomaterials*, 2005, **26**(21), 4383–4394.
23 H. Todo, Transdermal Permeation of Drugs in Various Animal Species, *Pharmaceutics*, 2017, **9**(3), 33–43.
24 J. A. Fairley and J. E. Rasmussen, Comparison of Stratum-Corneum Thickness in Children and Adults, *J. Am. Acad. Dermatol.*, 1983, **8**(5), 652–654.
25 K. Asaoka, J. Y. Bae and H. H. Lee, Porosity of dental gypsum-bonded investments in setting and heating process, *Dent. Mater. J.*, 2012, **31**(1), 120–124.
26 F. J. Verbaan, S. M. Bal, D. J. van den Berg, J. A. Dijksman, M. van Hecke and H. Verpoorten, *et al.*, Improved piercing of microneedle arrays in dermatomed human skin by an impact insertion method, *J. Controlled Release*, 2008, **128**(1), 80–88.
27 A. Arora, M. R. Prausnitz and S. Mitragotri, Micro-scale devices for transdermal drug delivery, *Int. J. Pharm.*, 2008, **364**(2), 227–236.
28 A. Kumar, X. Li, M. A. Sandoval, B. L. Rodriguez, B. R. Sloat and Z. Cui, Permeation of antigen protein-conjugated nanoparticles and live bacteria through microneedle-treated mouse skin, *Int. J. Nanomed.*, 2011, **6**, 1253–1264.
29 K. Matsuo, Y. Yokota, Y. Zhai, Y. S. Quan, F. Kamiyama and Y. Mukai, *et al.*, A low-invasive and effective transcutaneous immunization system using a novel dissolving microneedle array for soluble and particulate antigens, *J. Controlled Release*, 2012, **161**(1), 10–17.
30 N. Eliaz, *Degradation of Implant Materials*, Springer, New York, 2011.
31 H. S. Gill and M. R. Prausnitz, Coated microneedles for transdermal delivery, *J. Controlled Release*, 2007, **117**(2), 227–237.
32 M. F. Bachmann and G. T. Jennings, Vaccine delivery: a matter of size, geometry, kinetics and molecular patterns, *Nat. Rev. Immunol.*, 2010, **10**(11), 787–796.
33 E. Caffarel-Salvador and R. F. Donnelly, Transdermal Drug Delivery Mediated by Microneedle Arrays: Innovations and Barriers to Success, *Curr. Pharm. Des.*, 2016, **22**(9), 1105–1117.
34 M. C. Chen, K. Y. Lai, M. H. Ling and C. W. Lin, Enhancing immunogenicity of antigens through sustained intradermal delivery using chitosan microneedles with a patch-dissolvable design, *Acta Biomater.*, 2018, **65**, 66–75.
35 K. van der Maaden, E. M. Varypataki, S. Romeijn, F. Ossendorp, W. Jiskoot and J. Bouwstra, Ovalbumin-coated pH-sensitive microneedle arrays effectively induce ovalbumin-specific antibody and T-cell responses in mice, *Eur. J. Pharm. Biopharm.*, 2014, **88**(2), 310–315.

